Table 4. X-ray luminosity references.

Bibliographic reference	Telescope	Range [keV]	Size
Fabbiano et al. (1992)	*Einstein*	0.2−4	172
Brinkmann et al. (1994)	ROSAT	0.1−2.4	7
O'Sullivan et al. (2001)	ROSAT	0.1−17	83
Tajer et al. (2005)	ROSAT	0.1−2	10
Cappi et al. (2006)	XMM	0.2−10	16
David et al. (2006)	*Chandra*	0.5−2	8
Diehl & Statler (2007)	*Chandra*	0.3−5	7
Rosa González et al. (2009)	XMM	0.5−2	1
González-Martín et al. (2009)	*Chandra*	0.5−10	30
Akylas & Georgantopoulos (2009)	XMM	2−10	19
Grier et al. (2011)	*Chandra*	0.3−8	29
Brightman & Nandra (2011)	XMM	2−10	37
Liu (2011)	*Chandra*	0.3−8	147
Kim et al. (2019)	*Chandra*	0.5−5	12
		Total	256

Notes. The total number of sources (last line) is fewer than the sum of each sample size (last column). This is because the same sources were observed by different instruments. When it is the case, we keep the most recent estimate.

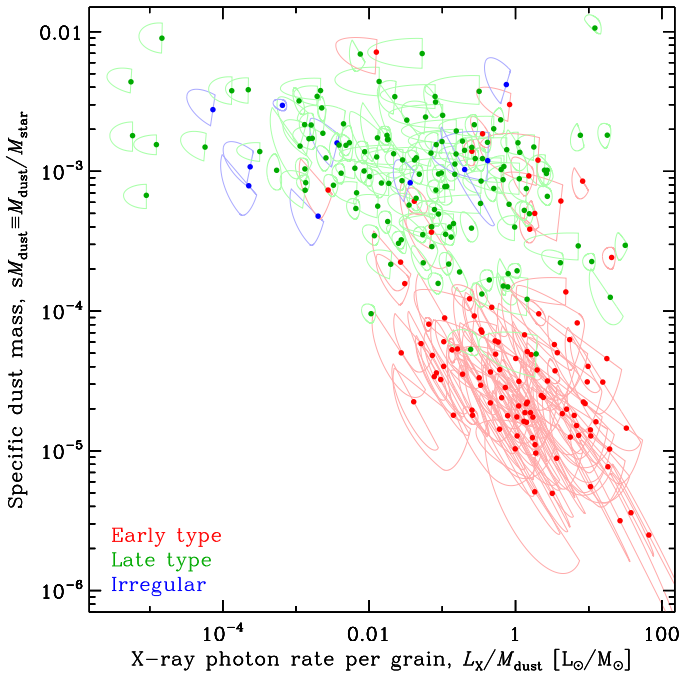

Fig. 9. Relation of dust mass to X-ray luminosity. This figure shows the variation of the dust-to-stellar mass ratio as a function of the X-ray photon rate per dust grain, for the sample of Table 4. This is a subset of the reference run (Sect. 3.2). The color convention is similar to Fig. 8. The Bayesian correlation coefficient of this relation is $\rho = -0.596^{+0.017}_{-0.015}$, with $CR_{95\%}(\rho) = [-0.62, -0.56]$.

galaxies. ETGs clearly lie in the bottom right quadrant of this figure. It is reminiscent of Fig. 10 in Smith et al. (2012), displaying L_{FIR}/L_B as a function of L_X/L_B.

We note there is however a significant intrinsic scatter in this relation. This could be due to the fact that most of the studies listed in Table 4 quote a total X-ray luminosity, including both: (i) point sources (AGNs, binary systems); and (ii) the diffuse thermal emission that is sole relevant to our case[16]. In addition, the spectral range used to compute the X-ray luminosity varies from one instrument to the other (Table 4), leading to systematic differences. Nonetheless, accounting for these differences, which is beyond the scope of this paper, would likely not change the plausibility that dust grains are significantly depleted in ETGs due to thermal sputtering.

4.1.3. On the variation of the dust-to-metal mass ratio

Panel d of Fig. 8 shows that the dustiness-metallicity relation is nonlinear. Rémy-Ruyer et al. (2014) first argued, relying on insights from the models of Asano et al. (2013) and Zhukovska (2014), that such a trend was the result of different dust production regimes: (i) at low 12 + log(O/H), dust production is dominated by condensation in type II Supernova (SN) ejecta, with a low yield; (ii) around a critical metallicity[17] of 12 + log(O/H) ≃ 8, grain growth in the ISM becomes dominant, causing a rapid increase of Z_{dust}; (iii) at high 12 + log(O/H), the dust production is dominated by grain growth in the ISM, with a yield about two orders of magnitude higher than SN II, and is counterbalanced by SN II blast wave dust destruction. Rémy-Ruyer et al. (2014) argued that the intrinsic scatter of the relation, which could not be explained by SED fitting uncertainties, was due to the fact that each galaxy has a particular star formation history (SFH). We explore this aspect in Sect. 5. In the following paragraphs, we discuss the different biases that could have induced an artificial nonlinearity in our empirical trend.

Comparison to DLAs. Figure 10 shows the evolution of the dust-to-metal mass ratio (DTM) as a function of metallicity. It is another way to look at the data in panel d of Fig. 8. A constant DTM corresponds to a linear dustiness-metallicity trend. The SUEs in Fig. 10 are not consistent with a constant DTM (horizontal yellow line). However, there are reports in the literature of objects exhibiting an approximately constant DTM, down to very low metallicities: damped Lyman-α absorbers (DLA). We have overlaid the DLA sample of De Cia et al. (2016). These measures are performed in absorption on redshifted systems, along the sightline of distant quasars. The metallicity and DTM are derived from a combination of atomic lines of volatile and refractory elements. We can see that the DLA DTMs vary significantly less than in our nearby galaxy sample[18]. Such an evolutionary behavior requires a high SN-dust condensation efficiency coupled to a weak grain growth rate in the ISM (e.g., De Vis et al. 2017a). Alternatively, the DLA estimates could be biased. It is indeed not impossible that the hydrogen column density of most DLAs includes dust- and element-free circumgalactic clouds in the same velocity range. It would result in a typical solar metallicity object appearing to have a solar DTM, and at the same time, an artificially lower metallicity, diluted by the additional pristine gas along the line of sight.

Accounting for the gas halo. The contamination of the gas mass estimate by external, dust- and element-poor gas is also

[16] David et al. (2006), Diehl & Statler (2007), Rosa González et al. (2009), and Kim et al. (2019) extract the thermal emission of the gas. We use these values for the sources in these catalogs.
[17] This is a concept introduced by Asano et al. (2013). Its exact value depends on the star formation history of each galaxy.
[18] We note that metallicities measured in absorption tend to always be lower than metallicities measured in emission (e.g., Hamanowicz et al. 2020).